An Improved Three-Level Neutral Point Clamped Converter System With Full-Voltage Balancing Capability for Bipolar Low-Voltage DC Grid

Bowei Li, *Graduate Student Member, IEEE*, Hao Tian, *Member, IEEE*, Li Ding, *Member, IEEE*, Xuesong Wu, *Member, IEEE*, Gregory J. Kish, *Senior Member, IEEE*, and Yunwei Ryan Li, *Fellow, IEEE*

***Abstract*—Bipolar low-voltage dc grids are an emerging and promising solution for power distribution. As a natural candidate for the distribution converter, the three-level neutral-point-clamped (3L-NPC) converter has inherent but limited capability in balancing the dc voltages during asymmetrical operation. This article begins by investigating the voltage balancing limits of the conventional 3L-NPC in detail. To overcome the identified limitations, an improved 3L-NPC converter system with a zigzag transformer and a neutral line is proposed. With the designed control strategy, the proposed converter system can provide full bipolar voltage balancing capability without extra devices or penalties on component ratings. The effectiveness and advantages of the proposed scheme are verified by simulation and experimental results.**

***Index Terms*—Asymmetrical operation, bipolar low-voltage dc (LVdc) grid, bipolar voltage balancing capability, three-level neutral point clamped (3L-NPC) converter.**

I. Introduction

BENEFITING from the evolving power electronics technology, as well as its inherent advantages, dc power is being increasingly utilized at different voltage levels [1]. The most recent emergence of dc is happening at low voltage level. With a growing share of distributed energy resources (DERs) and modern appliances relying on dc technology, low-voltage dc (LVdc) distribution is becoming an attractive concept as it requires fewer power conversion stages, leading to enhanced efficiency and reliability [2], [3].

There are two types of LVdc grids: unipolar and bipolar [4]. Compared with the simple two-wire unipolar configuration, the three-wire bipolar configuration is more promising as it provides two voltage levels, which leads to higher flexibility and reliability [5]. A typical bipolar LVdc grid is depicted in Fig. 1. A distribution transformer is used as an interface with the medium-voltage ac (MVac) grid. The distribution converter, as a crucial power electronics device, is responsible for power transfer between ac and dc sides as well as the construction of the split-dc bus.

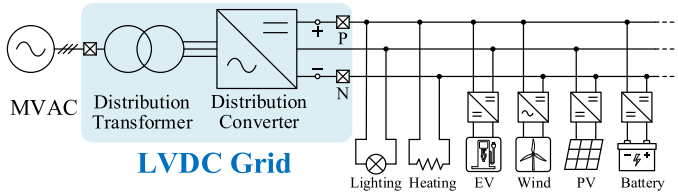

Fig. 1. Structure of a typical bipolar LVdc grid.

Asymmetrical operation is one of the main challenges for bipolar LVdc grids' applications. The asymmetry between dc poles caused by unbalanced loads or DERs may result in the problem of bipolar voltage imbalance, i.e., the dc voltages provided by two poles are unbalanced, which will deteriorate power quality and grid safety [6], [7]. The distribution converter is expected to accommodate this operational challenge. Therefore, the requirements for a distribution converter are: 1) bidirectional energy conversion, 2) split-dc bus structure, and 3) bipolar voltage balancing capability.

With its widely acknowledged versatility, efficiency, and reliability, the two-level voltage source converter (2L-VSC) has gained many applications for bipolar dc distribution. As Fig. 2(a) shows, two cascaded 2L-VSCs are used as the distribution converter to create the split-dc bus structure. With the independent control of two 2L-VSCs, the bipolar voltage balance can be readily and fully achieved, but this scheme brings excess cost and volume to the system. A single 2L-VSC lacks voltage balancing capability; therefore, adding additional circuitry is an option. A voltage balancer (VB) shown in Fig. 2(b) is deployed as the fourth leg of the 2L-VSC [8], which not only realizes the split-dc structure but also guarantees the voltage balance through drawing or injecting the unbalanced current between poles. Similarly, a dc current redistributor is proposed in [9], which can regulate the pole currents and, thus, balance the pole voltages.

As another common VSC with wide industry acceptance, the three-level neutral point clamped converter (3L-NPC) has more voltage levels, better harmonics performance, reduced voltage

Manuscript received 25 March 2023; revised 1 June 2023 and 26 July 2023; accepted 17 September 2023. Date of publication 22 September 2023; date of current version 23 October 2023. Recommended for publication by Associate Editor Z. Chen. *(Corresponding author: Bowei Li.)*

Bowei Li, Li Ding, Xuesong Wu, Gregory J. Kish, and Yunwei Ryan Li are with the Department of Electrical and Computer Engineering, University of Alberta, Edmonton, AB T6G 2R3, Canada (e-mail: bli4@ualberta.ca; lding@ualberta.ca; xuesong3@ualberta.ca; gkish@ualberta.ca; yunwei.li@ualberta.ca).

Hao Tian is with the School of Control Science and Engineering, Shandong University, Jinan 250061, China (e-mail: haotian@email.sdu.edu.cn).

Color versions of one or more figures in this article are available at https://doi.org/10.1109/TPEL.2023.3318531.

Digital Object Identifier 10.1109/TPEL.2023.3318531

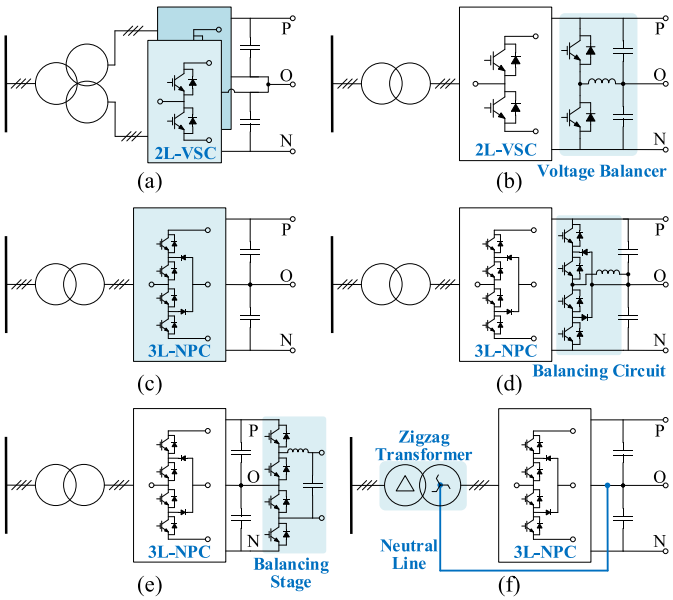

Fig. 2. Different schemes for bipolar LVdc grid. (a) Two cascaded 2L-VSCs for independent pole control. (b) Single 2L-VSC with VB. (c) Single conventional 3L-NPC converter. (d) Four-leg 3L-NPC converter. (e) Central 3L-NPC with additional balancing stage. (f) Proposed 3L-NPC converter system.

rating, lower switching frequency, and less power loss than the 2L-VSC [10], [11], [12]. Moreover, as shown in Fig. 2(c), the split-dc bus structure of 3L-NPC makes it a natural candidate for the distribution converter of bipolar LVdc grids.

Unlike the 2L-VSC, the 3L-NPC has inherent bipolar voltage balancing capability when feeding unbalanced dc-side loads. This capability has been studied extensively for the neutral point voltage balancing problem of the 3L-NPC inverter [13], [14], [15]. The corresponding methods are generally based on the same concept, i.e., adding the zero sequence voltage to the inverter output. This idea is realized by the injection of zero sequence modulation signals when using carrier-based pulsewidth modulation, or the manipulation of redundant small vectors for space vector modulation (SVM) [13]. In the context of bipolar LVdc grids, however, such control methods can only handle some range of asymmetries and cannot ensure the voltage balance under all the operating conditions. The voltage balance limits of 3L-NPC are analyzed under the SVM algorithm in [16], which indicates the limited voltage balance operation area of a single 3L-NPC.

Two kinds of balancing strategies have been proposed to extend the balanced operation area of the conventional 3L-NPC [2]. One is to make all the balancing efforts with the additional balancing circuit [16], which is also known as the four-leg 3L-NPC converter given in Fig. 2(d). The other is to adopt a coordinated balancing strategy between the 3L-NPC and the balancing stage [11], [17], [18]. As Fig. 2(e) shows, 3L dc–dc converters are used for voltage balancing when unbalanced power is out of the controllable area of the central NPC converter. However, both strategies require additional circuits or stages, which increase system costs, losses, or complexity.

Analysis carried out in Section II will show that the inherent voltage balancing capability of Fig. 2(c) becomes severely limited for large values of modulation index. To overcome this roadblock while preventing excessive cost, this article proposes an improved 3L-NPC converter system, as depicted in Fig. 2(f). Compared to Fig. 2(c) with a conventional grid-interfacing transformer, the proposed scheme gains full bipolar voltage balancing capability by exploiting a zigzag transformer connection. In contrast with Fig. 2(d) and (e), the proposed scheme does not require the addition of any extra devices. It is important to note that the grid-interfacing transformer is already an essential part of the overall system, as depicted in Fig. 1. Therefore, the use of a zigzag transformer does not impose any additional system-level complexity. The contribution of this article is twofold.

1) A detailed analysis is carried out to derive the voltage balance operation area of the conventional 3L-NPC under sinusoidal pulsewidth modulation (SPWM) strategy, considering its popularity and wide application in the industry. The limited bipolar voltage balancing capability of the conventional 3L-NPC converter is elaborated.
2) An improved 3L-NPC converter system with a zigzag transformer and a neutral line is proposed for bipolar LVdc grid applications. Based on the idea of manipulating the zero sequence current, the proposed converter system acquires full bipolar voltage balancing capability without adding any extra devices or having any penalty on component ratings. The designed control strategy can ensure the voltage balance under all the dc load conditions.

The rest of this article is organized as follows. Section II first studies the midpoint current of 3L-NPC in detail. The required current to keep the dc voltage balance is then analyzed, and the voltage balance operation area of 3L-NPC is depicted to clarify the limitation of the conventional scheme. In Section III, a new scheme is proposed for a bipolar LVdc grid, whose full-voltage balancing capability is explained by analysis results. Then controllers are designed to regulate the dc-link voltage and realize the voltage balancing. Simulation and experimental results are presented in Section IV to verify the effectiveness and advantages of the proposed scheme. Finally, Section V concludes this article.

II. Limited Bipolar Voltage Balancing Capability of the Conventional 3L-NPC

A. Bipolar LVDC Grid Based on a Conventional 3L-NPC

The bipolar LVdc grid based on a conventional 3L-NPC converter is presented in Fig. 3. A single 3L-NPC is interfaced to the MVAC grid through a three-phase two-winding transformer and an L filter. The split dc-link capacitors naturally form the three-wire structure with two dc poles, i.e., the positive pole (P) and the negative pole (N). The neutral point of 3L-NPC is connected to the neutral terminal (O) of the LVdc grid, referred to as the midpoint in this analysis.

It is known that the bipolar voltage imbalance can be solved by properly controlling the current flowing through the midpoint [9]. Hence, the midpoint current of 3L-NPC will be investigated in detail. Then, with the analysis of the unbalanced dc side, the limited bipolar voltage balancing capability of Fig. 3 will be clarified.

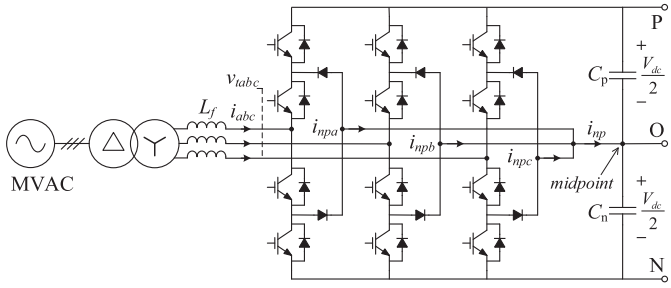

Fig. 3. Bipolar LVdc grid based on a conventional 3L-NPC converter.

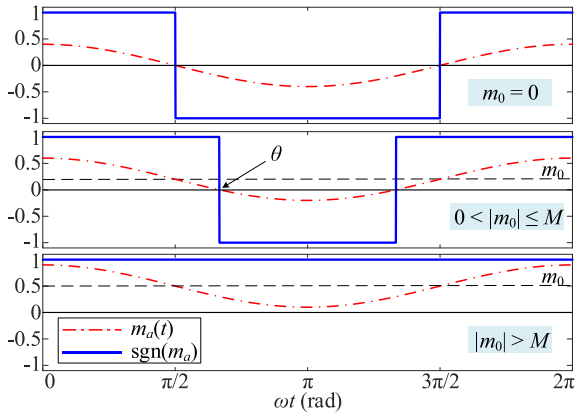

Fig. 4. Illustration of $m_a(t)$ and sgn(m_a) for different m_0.

B. Midpoint Current of 3L-NPC

For a three-phase 3L-NPC using the SPWM strategy, the averaged ac terminal voltage of phase j ($j = a, b, c$) is

$$v_{tj}(t) = m_j(t)\frac{V_{\rm dc}}{2} \tag{1}$$

where $V_{\rm dc}$ is the dc-link voltage, and $m_j(t)$ is the modulation signal for phase j

$$m_j(t) = M\cos(\omega t + \theta_j) + m_0 \tag{2}$$

where M is the modulation index; ω and θ_j are the angular frequency and initial phases of modulation signals. θ_j = [0, -2π/3, 2π/3] for $j = a, b, c$. m_0 is the injected zero sequence modulation signal, which can be manipulated to provide inherent bipolar voltage balancing capability for the 3L-NPC.

AC-side currents of the 3L-NPC are expressed as

$$i_j(t) = I_m\cos(\omega t + \theta_j - \varphi) \tag{3}$$

where I_m is the peak amplitude of ac current, φ is the angle of current lagging the voltage, and cosφ is the power factor.

After applying the switching function and average operator [19], the averaged current flowing into the midpoint from phase j is derived as

$$i_{npj}(t) = (1 - |m_j(t)|)\, i_j(t). \tag{4}$$

According to Fig. 3, the midpoint current i_{np} is the sum of i_{npj}. Assuming the three-phase currents are balanced i.e., $i_a(t) + i_b(t) + i_c(t) = 0$, then

$$i_{np}(t) = -\sum_{j=a,b,c} |m_j(t)|\, i_j(t). \tag{5}$$

To further simplify i_{np}, taking phase a as an example, let

$$f_a(t) = |m_a(t)|\, i_a(t) = m_a(t) i_a(t) \mathrm{sgn}(m_a) \tag{6}$$

where the function sgn(·) is defined as

$$\mathrm{sgn}(x) = \begin{cases} 1, & x > 0 \\ 0, & x = 0 \\ -1, & x < 0 \end{cases}. \tag{7}$$

Based on (2) and (3), $m_a(t)\cdot i_a(t)$ can be written as the sum of dc, fundamental, and double frequency components

$$m_a(t)i_a(t) = \frac{MI_m}{2}\cos\varphi + m_0 I_m\cos(\omega t - \varphi) + \frac{MI_m}{2}\cos(2\omega t - \varphi). \tag{8}$$

Also, sgn(m_a) can further be simplified depending on the value of injected m_0. For three cases of m_0, the corresponding $m_a(t)$ and sgn(m_a) are illustrated in Fig. 4.

When $|m_0| > M$, sgn(m_a) is a constant

$$\mathrm{sgn}(m_a) = 1 \cdot \mathrm{sgn}(m_0). \tag{9}$$

Considering only the dc component of the midpoint current can be used for bipolar voltage balancing, synthesize (6)–(9) and denote F_a as the dc component of $f_a(t)$

$$F_a = \frac{I_m\cos\varphi}{2} M\mathrm{sgn}(m_0). \tag{10}$$

The result shown in (10) also holds for phases b and c. Based on (5), the dc component of the midpoint current is

$$I_{np} = \frac{-3I_m\cos\varphi}{2} M\mathrm{sgn}(m_0). \tag{11}$$

On the other hand, when $|m_0| \le M$, as shown in Fig. 4, sgn(m_a) is a periodic function, which can be expanded by using the Fourier series

$$\mathrm{sgn}(m_a) = \frac{2}{\pi}\left(\theta - \frac{\pi}{2}\right) + \frac{4}{\pi}\sum_{k=1}^{\infty}\frac{1}{k}\sin(k\theta)\cos(k\omega t) \tag{12}$$

where $\theta = \cos^{-1}(-m_0/M)$.

Let $\lambda = 2/\pi*(\theta-\pi/2)$. Note that $\lambda = 0$ if $m_0 = 0$, which means there is no dc component in sgn(m_a) or i_{np}.

When substituting (6) into (8) and (12), the following relationship can be derived:

$$f_a(t) = f_{a1}(t) + f_{a2}(t) + f_{a3}(t) \tag{13}$$

where

$$f_{a1}(t) = \frac{MI_m}{2}\left[\lambda\cos\varphi + \lambda\cos(2\omega t - \varphi)\right] + \frac{2MI_m}{\pi}\cos\varphi\sum_{k=1}^{\infty}\frac{1}{k}\sin(k\theta)\cos(k\omega t)$$

$$f_{a2}(t) = \frac{MI_m}{\pi}\sum_{k=1}^{\infty}\frac{1}{k}\sin(k\theta)\cos[(k+2)\omega t - \varphi]$$

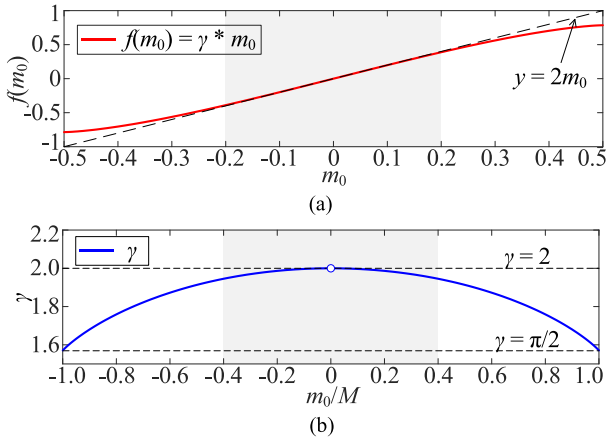

Fig. 5. Illustration of $f(m_0)$ and its slope γ. (a) Approximate linear characteristic of $f(m_0)$. (b) Range of γ ($m_0 \in$ [-0.5, 0.5], $M = 0.5$).

$$+\frac{MI_m}{\pi}\sum_{k=1}^{\infty}\frac{1}{k}\sin(k\theta)\cos[(k-2)\omega t+\varphi]$$

$$f_{a3}(t)=m_0 I_m\lambda\cos(\omega t-\varphi)+\frac{2m_0 I_m}{\pi}\sum_{k=1}^{\infty}\frac{1}{k}\sin(k\theta)$$
$$\times\{\cos[(k+1)\omega t-\varphi]+\cos[(k-1)\omega t+\varphi]\}.$$

It can be seen that $f_a(t)$ is composed of dc and many frequency components, which respectively correspond to the dc current and harmonics of i_{npa}.

By leaving out all the sinusoidal quantities of (13), the dc component of $f_a(t)$ can be calculated as

$$F_a=\frac{I_m\cos\varphi}{\pi}f(m_0) \tag{14}$$

where $f(m_0)$ is defined as

$$f(m_0)=\left(\frac{\theta-\pi/2}{\sin(\theta-\pi/2)}+\sin\theta\right)m_0. \tag{15}$$

Since i_{npa}, i_{npb}, and i_{npc} have the same dc component, according to (5), the resulting dc component of the 3L-NPC midpoint current is

$$I_{np}=\frac{-3I_m\cos\varphi}{\pi}f(m_0). \tag{16}$$

For specific operating currents and power factors, I_{np} relates to the injected m_0. It is interesting to demonstrate this relationship through the illustration of $f(m_0)$. As shown in Fig. 5(a), for a large domain of m_0, $f(m_0)$ shows an approximate linear characteristic. It is very close to the line of $y = 2m_0$, especially when $|m_0|$ is small. These are explained by plotting the slope of $f(m_0)$, denoted as γ. When $|m_0/M| \in [-0.4, 0.4]$, as the shaded area of Fig. 5(b), the slope is approximately at its maximum, $\gamma \approx 2$. When $|m_0| = M$, the minimum slope $\gamma = \pi/2$.

To counteract the dc voltage drift under slightly unbalanced loads, the required m_0 is very small relative to M, and the relationship between I_{np} and m_0 is usually treated as linear [19]. For more severe cases of bipolar voltage imbalance, where the required m_0 is large and the linear relationship no longer holds, (15) and (16) can be used to obtain a more accurate value of m_0.

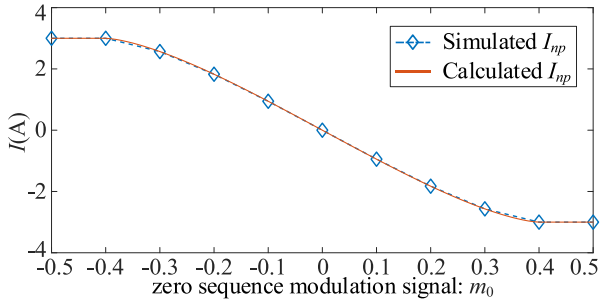

Fig. 6. Relationship between I_{np} and m_0 ($M = 0.4$, $I_m = 10$ A, $\varphi = \pi/3$).

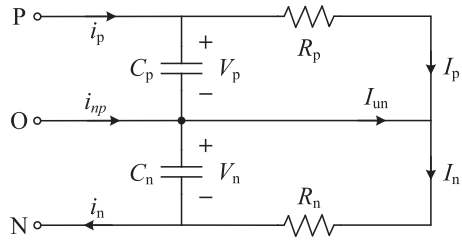

Fig. 7. DC-side analysis circuit of a bipolar LVdc grid.

Based on the preceding analysis, the relationship between I_{np} and injected m_0 can be precisely obtained. For $M = 0.4$, $I_m = 10$ A, $\varphi = \pi/3$, the simulated and calculated I_{np} under different m_0 are presented in Fig. 6. An approximately negative linear relationship can be observed for $|m_0| \le M$, whereas when $|m_0| > M$, I_{np} will be fixed at the limit values. Moreover, it can be seen that the calculated results based on equations are in good agreement with simulation results, which verifies the correctness of (11) and (16).

C. Voltage Balance Operation Area of 3L-NPC

For a bipolar LVdc grid, the analysis circuit used for the dc-side asymmetrical operation is given in Fig. 7. For convenience, the asymmetry between two dc poles is represented by two unbalanced load resistors, i.e., R_p and R_n.

Assume the unbalanced load condition is represented by

$$R_p=\varepsilon R_n \tag{17}$$

with unbalanced degree $\varepsilon \in (0, +\infty)$. Note that $\varepsilon = 1$ represents the balanced dc load condition.

The pole voltages are expressed as

$$V_p=I_p R_p \tag{18}$$
$$V_n=I_n R_n. \tag{19}$$

Assume the pole voltages could keep balanced after injecting m_0, i.e., $V_p = V_n = V_{dc}/2$. Then the pole currents satisfy

$$I_n=\varepsilon I_p. \tag{20}$$

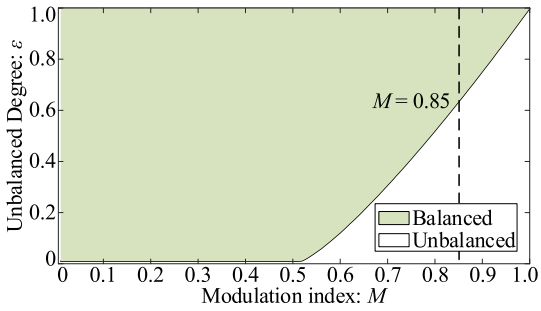

Fig. 8. Voltage balance operation area of 3L-NPC utilizing SPWM.

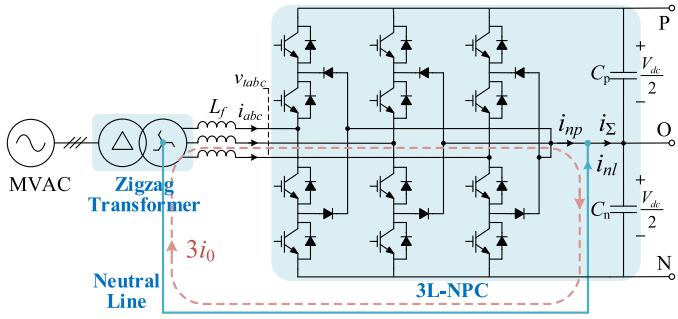

Fig. 9. Improved 3L-NPC converter system for bipolar LVdc grid.

Similarly, the power consumed by the negative pole is proportional to that of the positive pole

$$P_{\mathrm{n}} = \varepsilon P_{\mathrm{p}}. \tag{21}$$

The total power demanded by the dc side is

$$P_{\mathrm{dc}} = \frac{V_{\mathrm{dc}}}{2} I_{\mathrm{p}} \left(1+\varepsilon\right). \tag{22}$$

The power transmitted from the ac side is

$$P_{\mathrm{ac}} = \sum_{j=a,b,c} \frac{1}{T} \int_0^T v_{tj}(t) i_j(t) dt. \tag{23}$$

Substituting (1)–(3) into (23)

$$P_{\mathrm{ac}} = \frac{3}{4} M V_{\mathrm{dc}} I_m \cos\varphi. \tag{24}$$

Neglecting the converter losses, i.e., $P_{\mathrm{ac}} = P_{\mathrm{dc}}$, yields

$$I_{\mathrm{p}} = \frac{3}{2\left(1+\varepsilon\right)} M I_m \cos\varphi. \tag{25}$$

To maintain the voltage balance of the two poles, the required unbalanced current from the neutral terminal is

$$I_{\mathrm{un}} = I_{\mathrm{n}} - I_{\mathrm{p}} = \left(\varepsilon - 1\right) I_{\mathrm{p}}. \tag{26}$$

Let the midpoint current of 3L-NPC supply the required current, i.e., $I_{np} = I_{\mathrm{un}}$. Then, substituting (16) into (25) and (26), the final equation is expressed as

$$\frac{\pi}{2} \frac{1-\varepsilon}{1+\varepsilon} M = \left(\frac{\theta - \pi/2}{\sin\left(\theta - \pi/2\right)} + \sin\theta \right) m_0. \tag{27}$$

For any given M and ε, the required m_0 can be decided by (27). Considering the right-hand side of (27) is not in analytical form, a numerical solution can be found using MATLAB. If the obtained m_0 leads to overmodulation, i.e., $m_0 + M > 1$, which means the demand of I_{un} exceeds the normal limit of I_{np}, the bipolar voltage balancing capability of 3L-NPC would be regarded as insufficient to guarantee the voltage balance. Based on this constraint and (27), the voltage balance limits of 3L-NPC can be determined.

For $\varepsilon \in (0, 1]$, the voltage balance operation area of the 3L-NPC using SPWM is plotted in Fig. 8, where a distinct relationship between ε and M can be observed. When $M \leq 0.5$, the available I_{np} can reach the maximum required amount without causing overmodulation; therefore, voltage balance can be theoretically realized even for a very small ε. However, when $M > 0.5$, the allowable ε for balanced operation gradually decreases with increasing M. Fig. 8 shows that the inherent bipolar voltage balancing capability of the 3L-NPC is dependent on M and becomes very limited when M is large.

III. Proposed 3L-NPC Converter System and Control Strategy for Bipolar LVDC Grid

A. Improved 3L-NPC Converter System

The analysis in Section II, culminating in the plot of Fig. 8, shows that the conventional 3L-NPC has very limited bipolar voltage balancing capability for large modulation index values (e.g., $M > 0.85$). To overcome this limitation, Fig. 9 proposes an improved 3L-NPC converter system with full bipolar voltage balancing capability for bipolar LVdc grid applications. This scheme still adopts a single 3L-NPC as the distribution converter; however, instead of using additional devices, only a neutral line is added between the neutral point of the transformer and the midpoint of the dc side.

As previously mentioned, the inherent bipolar voltage balancing capability of 3L-NPC is based on adding zero sequence voltage, which is realized by modifying modulation strategies, e.g., injecting zero sequence modulation signals for SPWM. In contrast, the proposed 3L-NPC converter system acquires full-voltage balancing capability by adding zero sequence current. Overall, this idea is realized by 1) using a zigzag transformer, 2) creating a current path, i.e., a neutral line, and 3) the proper control of zero sequence current.

B. Features of Zigzag Transformer

As a key device, a zigzag transformer replaces the traditional transformer as the distribution transformer of the bipolar LVdc grid. The connection and phasor diagrams of a delta-zigzag transformer are given in Fig. 10.

The primary-side windings are connected in delta to provide a circulation path for third harmonic currents. The secondary-side windings are in a zigzag connection to provide low impedance to zero sequence currents. Specifically, when zero sequence current exists in three phases, it will flow through two segmented windings of each phase in opposite directions, then the zero sequence magnetic flux will be canceled with each other in each limb. Therefore, the zigzag connection on the secondary side

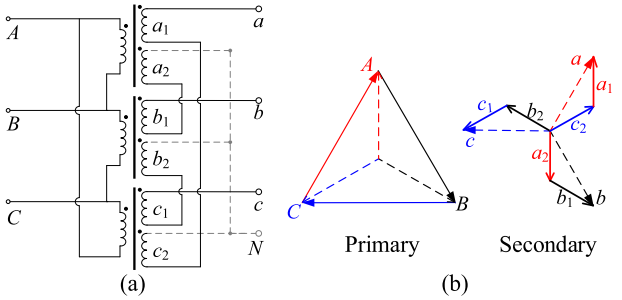

Fig. 10. Delta-zigzag transformer. (a) Connection diagram. (b) Phasor diagram.

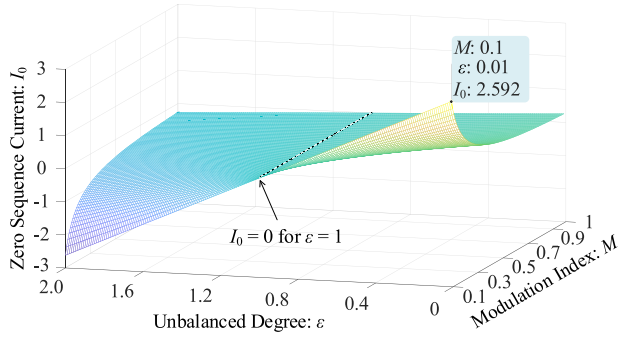

Fig. 11. Required I_0 for given ε and M ($\varepsilon \in (0, 2]$, M$\in$ [0.1, 1]).

can prevent the transformer saturation problem caused by the zero sequence current.

C. Analysis of Full-Voltage Balancing Capability

Since the improved 3L-NPC converter in Fig. 9 is based on the injection of zero sequence current rather than zero sequence modulation signal, (2) and (3) are modified as

$$m_j(t) = M\cos(\omega t + \theta_j) \tag{28}$$

$$i_j(t) = I_m\cos(\omega t + \theta_j - \varphi) + i_0 \tag{29}$$

where i_0 is the zero sequence current flowing in each phase.

Only the zero sequence components of $i_j(t)$ can flow through the neutral point of a zigzag transformer, so the neutral line current is

$$i_{nl} = -3i_0. \tag{30}$$

According to (4), the midpoint current for Fig. 9 is now

$$i_{np}(t) = 3i_0 - \sum_{j=a,b,c} |m_j(t)| \cdot i_j(t). \tag{31}$$

Take phase a as an example, the relationship in (6) still holds, but the product of $m_a(t)$ and $i_a(t)$ becomes

$$m_a(t)i_a(t) = \frac{MI_m}{2}\left[\cos\varphi + \cos(2\omega t - \varphi)\right] + Mi_0\cos\omega t. \tag{32}$$

With $m_0 = 0$, sgn(m_a) is derived from (12)

$$\mathrm{sgn}(m_a) = \frac{4}{\pi}\sum_{k=1}^{\infty}\frac{1}{k}\sin\left(\frac{k\pi}{2}\right)\cos(k\omega t). \tag{33}$$

Substituting (6) into (32) and (33)

$$f_a(t) = f_{a1}(t) + f_{a2}(t) + f_{a3}(t) \tag{34}$$

where

$$f_{a1}(t) = \frac{2MI_m}{\pi}\cos\varphi\sum_{k=1}^{\infty}\frac{1}{k}\sin\left(\frac{k\pi}{2}\right)\cos(k\omega t)$$

$$f_{a2}(t) = \frac{MI_m}{\pi}\sum_{k=1}^{\infty}\frac{1}{k}\sin\left(\frac{k\pi}{2}\right)\cos[(k+2)\omega t - \varphi] + \frac{MI_m}{\pi}\sum_{k=1}^{\infty}\frac{1}{k}\sin\left(\frac{k\pi}{2}\right)\cos[(k-2)\omega t + \varphi]$$

$$f_{a3}(t) = \frac{2Mi_0}{\pi}\sum_{k=1}^{\infty}\frac{1}{k}\sin\left(\frac{k\pi}{2}\right)\cos[(k+1)\omega t] + \frac{2Mi_0}{\pi}\sum_{k=1}^{\infty}\frac{1}{k}\sin\left(\frac{k\pi}{2}\right)\cos[(k-1)\omega t].$$

Only $f_{a3}(t)$ has a dc component when $k = 1$, so the dc component of $f_a(t)$ is calculated as

$$F_a = \frac{2M}{\pi}i_0. \tag{35}$$

This result also holds for phases b and c. According to (31), the dc component of the midpoint current i_{np} in Fig. 9 is

$$I_{np} = \left(3 - \frac{6M}{\pi}\right)i_0. \tag{36}$$

Applying KCL at the dc terminal in Fig. 9 yields

$$i_{nl} + i_{np} = i_\Sigma \tag{37}$$

where i_Σ is the total current provided by the proposed 3L-NPC converter system with a dc value

$$I_\Sigma = -\frac{6M}{\pi}I_0. \tag{38}$$

Here, only the dc component of i_0 (i.e., I_0) is considered.

On the other hand, since the dc load condition does not change, the required unbalanced current to keep dc voltage balance remains as (26). Letting $I_\Sigma = I_{\mathrm{un}}$, based on (18), (26), and (38), the final equation is obtained as

$$I_0 = \frac{\pi}{12}\frac{V_{\mathrm{dc}}}{R_{\mathrm{p}}M}(1 - \varepsilon). \tag{39}$$

For any given M and ε, the required I_0 in Fig. 9 can be determined from (39) as long as V_{dc} and R_{p} are known. For example, assuming $V_{\mathrm{dc}}/R_{\mathrm{p}} = 1$ A, the corresponding relationship between M, ε, and I_0 is illustrated in Fig. 11.

Considering that I_0 is technically unlimited, the improved 3L-NPC converter system in Fig. 9 is able to ensure balanced dc-side voltages under all possible load conditions, i.e., having full bipolar voltage balancing capability.

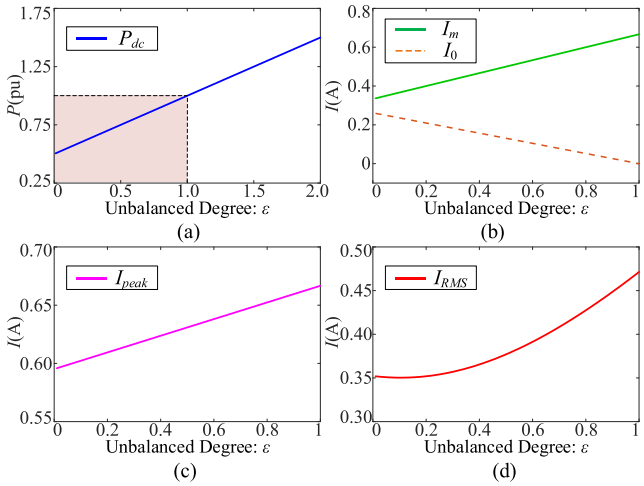

Fig. 12. Graphs of (22) and (39)–(42) for current stress analysis. (a) $P_{\rm dc}$ versus ε. (b) I_m and I_0 versus ε. (c) $I_{\rm peak}$ versus ε. (d) $I_{\rm RMS}$ versus ε.

D. Analysis of Component Ratings

This section analyzes the impact of injecting zero sequence dc currents on the ratings needed for the semiconductor switches, interface inductors, and transformer windings in Fig. 9. It will be shown that these components do not experience any increased current stresses in comparison to the conventional system given by Fig. 3.

From (18), (22), and (24), neglecting the converter losses and assuming the unity power factor and unity modulation index, the ac current peak amplitude is expressed as

$$I_m = \frac{V_{\rm dc}\,(1+\varepsilon)}{3R_P}. \tag{40}$$

Considering the dc component of injected current given by (39), the peak current and RMS current flowing through the inductors and converter-side windings are calculated as

$$I_{\rm peak} = I_m + I_0 \tag{41}$$

$$I_{\rm RMS} = \sqrt{I_m^2/2 + I_0^2}. \tag{42}$$

To further analyze the component ratings, the maximum values of $I_{\rm peak}$ and $I_{\rm RMS}$ can be determined from (41) and (42) as long as $V_{\rm dc}$ and $R_{\rm p}$ are known. Assuming $V_{\rm dc}/R_{\rm p} = 1$ A, the graphs based on (22) and (39)–(42) are depicted in Fig. 12.

It should be noted that $P_{\rm dc}$ will exceed 1.0 per unit when $\varepsilon > 1$, as shown in Fig. 12(a). That is, if $\varepsilon > 1$, the dc loading becomes excessive such that the required $P_{\rm dc}$ will exceed the designed capacity of the system. Therefore, to avoid this unwanted scenario, the unbalanced degree is limited to $\varepsilon \in (0, 1]$ for the subsequent analysis. Recall that $\varepsilon = 1$ denotes a balanced load condition, as given by (17).

When the dc-side loads become unbalanced, the required dc balancing current increases but the ac terminal current decreases compared to the balanced situation due to the reduced total dc-side power [20], [21]. This point is well demonstrated in Fig. 12(b), where I_0 increases but I_m decreases for reduced ε and $P_{\rm dc}$. As a result, Fig. 12(c) and (d) validate that the maximum peak and RMS currents occur at the balanced condition ($\varepsilon = 1$), which are also the maximum values for the conventional scheme in Fig. 3.

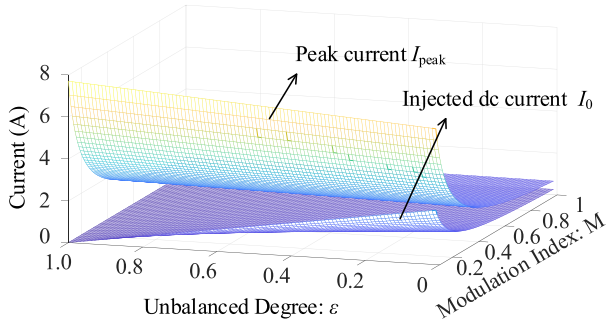

Fig. 13. Comparison of $I_{\rm peak}$ and I_0 for given ε and M ($\varepsilon \in (0, 1]$, M$\in$ [0.1, 1]).

TABLE I
COMPARISON OF SCHEMES FOR BIPOLAR DC DISTRIBUTION

	Conventional scheme [see Fig. 2(c)]	VB-based scheme [see Fig. 2(d)]	Proposed scheme [see Fig. 2(f)]
Capital cost	Low	High	Medium
Losses	Low	High	Low
Control complexity	Low	High	Low
Full bipolar voltage balancing capability	No	Yes	Yes

Based on the above analysis, even though the proposed converter system in Fig. 9 introduces a zero sequence dc current that flows through the switches, interface inductors, and transformer converter-side windings, the ratings of these components can still be designed the same as the conventional scheme. In other words, there is no penalty in terms of increased component ratings for the proposed scheme.

A comparison of $I_{\rm peak}$ and I_0 is illustrated in Fig. 13. Observe the injected dc current is relatively small compared to the overall peak current for the proposed scheme. This implies that there is little concern about inductor saturation in practice.

To further clarify the advantages of the proposed scheme in Fig. 2(f) to the conventional scheme [see Fig. 2(c)] and VB-based scheme [e.g., Fig. 2(d)], a basic qualitative comparison is summarized in Table I. Since there is no penalty for increased current stress after the injection of zero sequence current, as well as the elimination of zero sequence voltage, the losses of the proposed scheme are considered to be low. The capital cost will increase a little because the manufacturing cost of the zigzag transformer would be higher than that of the conventional transformer due to its more complicated winding connection [20]. However, it can enable a full bipolar voltage balancing capability of a single 3L-NPC without adding extra devices to the previous system, which makes sure that the proposed scheme has lower cost, losses, and control complexity compared to the VB-based scheme.

E. Controller Design

A control strategy is designed for the proposed 3L-NPC converter system of Fig. 9, and its block diagram is shown in

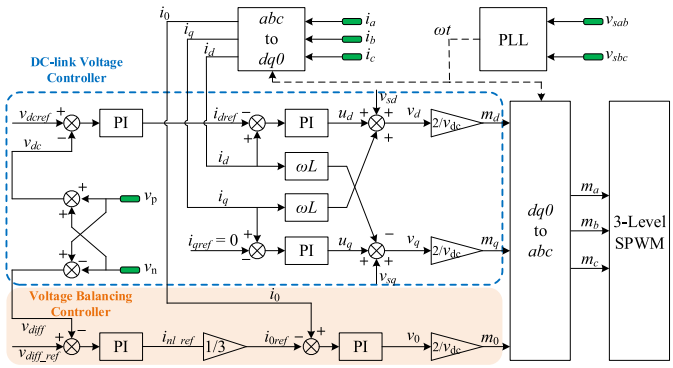

Fig. 14. Block diagram of the designed control strategy for the proposed 3L-NPC converter system.

Fig. 14. $v_{\rm p}$ and $v_{\rm n}$ are the measured pole voltages, while $v_{\rm dc}$ and $v_{\rm diff}$ represent the corresponding sum and difference quantities.

There are two main control objectives. The first is to regulate $v_{\rm dc}$ at its reference $v_{\rm dcref}$. A classic double-loop controller built in the *dq*-frame is used as the dc-link voltage controller. The second objective is achieving dc-side voltage balancing according to the mechanism described in Section III-C. Unlike the voltage-mode controller for solving the neutral point voltage balancing problem of the conventional 3L-NPC inverter [15], [19], the proposed voltage balancing controller adopts current-mode control due to its superior dynamic performance and higher control precision [22].

As shown in Fig. 14, the voltage balancing controller has two control loops. The outer loop compares $v_{\rm diff}$ with its reference ($v_{\rm diff\_ref} = 0$) and outputs a command for neutral line current ($i_{\rm nl\_ref}$), which is divided by 3 to obtain the reference value for zero sequence current ($i_{0\rm ref}$). The inner loop compares $i_{0\rm ref}$ with i_0 and outputs a zero sequence control signal (v_0). Both loops are implemented by PI controllers. Zero sequence modulation signal m_0 is generated to regulate i_0. However, the required m_0 is very small. The dynamics of i_0 are described by

$$\frac{di_0}{dt} = \frac{1}{L_f} m_0 \frac{V_{\rm dc}}{2} \tag{43}$$

where L_f is the ac-side filter inductance in Fig. 9.

At a steady state, m_0 becomes a constant

$$I_0 R_{\rm para} = m_0 \frac{V_{\rm dc}}{2} \tag{44}$$

where $R_{\rm para}$ represents the total parasitic resistance of the inductors and switches. The dc voltage drop caused by $R_{\rm para}$ is very small compared to $V_{\rm dc}$; therefore, the required m_0 is practically negligible, i.e., $m_0 \approx 0$.

IV. Verification Studies

A. Simulation Results

1) Comparison of Conventional and Proposed Schemes: To verify the effectiveness and advantages of the proposed scheme, the 3L-NPC converters in Figs. 3 and 9 are modeled in MATLAB/Simulink. For convenience, they are named scheme 1 and scheme 2, respectively. Both schemes are simulated based on the parameters in Table II.

TABLE II
Simulation Parameters

Parameter	Value	Parameter	Value
Grid RMS line voltage	5 kV	DC-link voltage	800 V
Grid frequency	60 Hz	Switching frequency	5 kHz
Transformer turns ratio	20 : 1 or 12.5 : 1	DC loads ($R_{\rm p}$ & $R_{\rm n}$)	20 and 50 Ω or 50 Ω and ∞
L filter inductance	6 mH	Capacitance per pole	4 mF

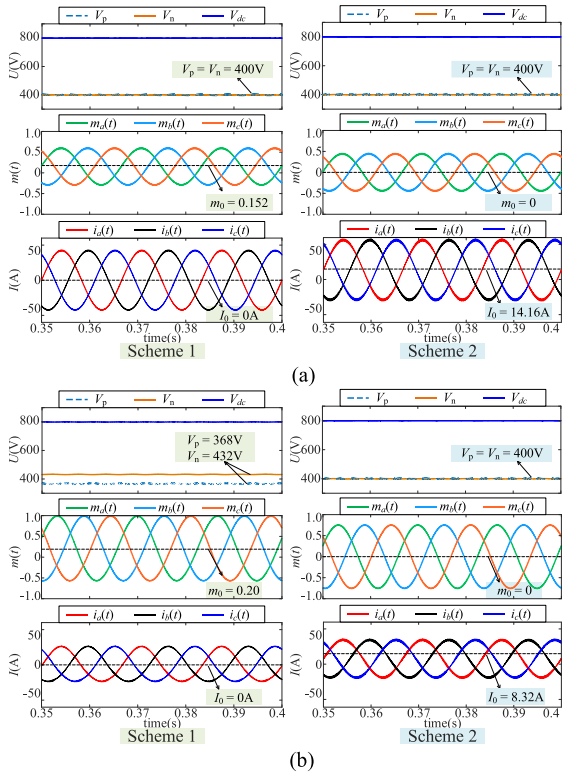

Fig. 15. Simulation waveforms to compare two 3L-NPC schemes. (a) Low modulation index ($M = 0.45$). (b) High modulation index ($M = 0.76$).

The dc-side voltage balancing mechanisms of the two schemes are demonstrated first. The dc load condition is set as $R_{\rm p} = 20\ \Omega$, $R_{\rm n} = 50\ \Omega$ ($\varepsilon = 0.4$). As shown in Fig. 15(a), when the system operates under a low modulation index ($M = 0.45$), both schemes can realize the balanced pole voltages. Scheme 1 is based on the injection of zero sequence modulation signal ($m_0 = 0.152$), while scheme 2 is based on the injection of zero sequence current ($I_0 = 14.16$ A).

However, when the modulation index is high ($M = 0.76$), as shown in Fig. 15(b), scheme 1 can no longer keep the voltage balance between the two poles. This is because the required m_0 for voltage balancing is larger with a higher M, as dictated by (27). Consequently, the injected m_0 is insufficient to realize bipolar voltage balance due to the risk of overmodulation. This is the drawback of traditional scheme 1.

In contrast, scheme 2 can maintain voltage balancing as the injected I_0 is technically unlimited. The required I_0 is inversely

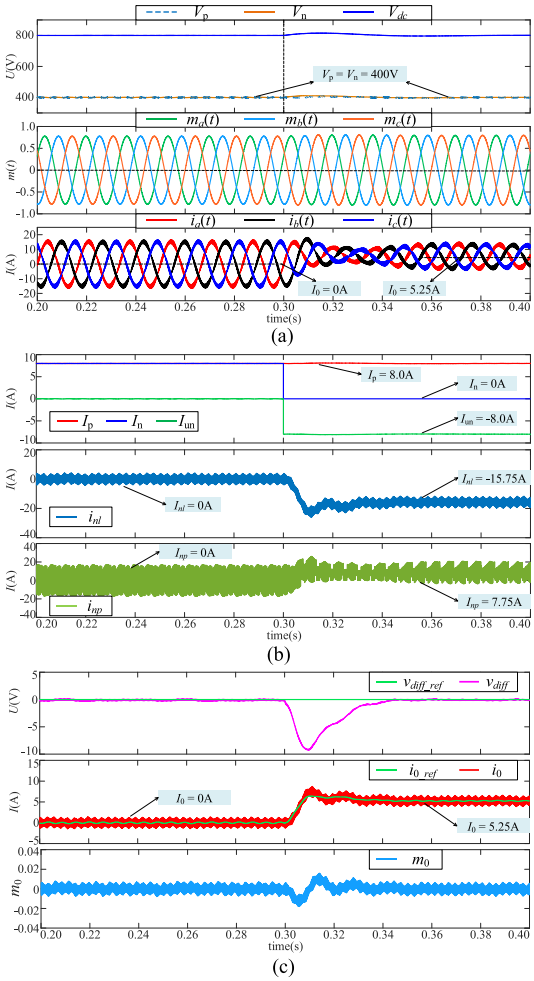

Fig. 16. Simulation waveforms to verify full-voltage balancing capability. (a) DC-side voltages, modulation signals, and ac-side currents. (b) Current waveforms. (c) Dynamic performance of the controller.

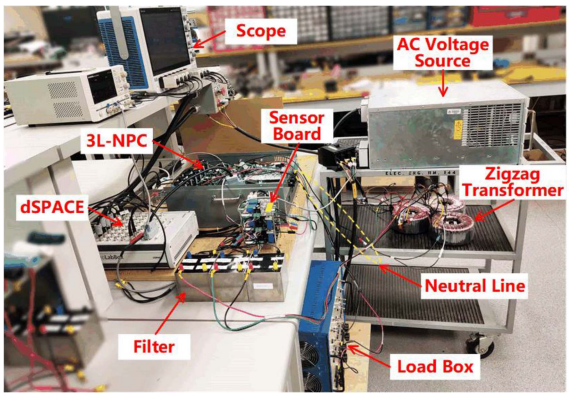

Fig. 17. Experimental setup.

proportional to M, as implied by (39), and the simulated values of I_0 are in good agreement with the theoretical values. Besides, it is noticed that scheme 2 has a lower ac current quality than scheme 1. This is because the injection of i_0 also brings common mode switching harmonics besides I_0, which can be suppressed through improved modulation strategies, but are not the focus of this article.

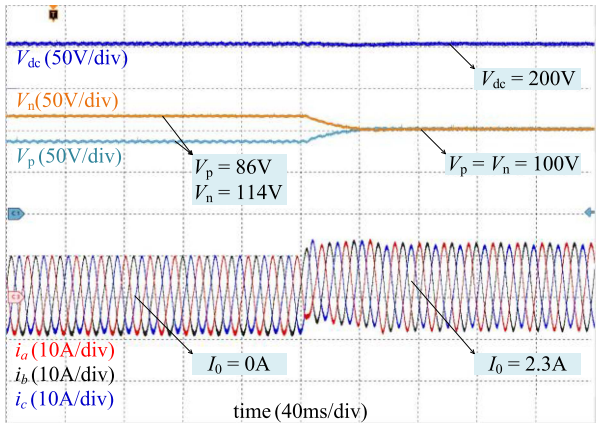

Fig. 18. Experimental waveforms of scenario 1.

2) Full Bipolar Voltage Balancing Capability: The proposed scheme has full bipolar voltage balancing capability due to its zero sequence current injection mechanism. This capability is reflected not only in the avoidance of limitations on M but also in arbitrary load conditions, i.e., it can balance pole voltages even for completely unbalanced dc loads.

The proposed system in Fig. 9 is first simulated under balanced loads ($R_p = R_n = 50\ \Omega$, $\varepsilon = 1$), and then the load on the negative pole is removed at $t = 0.3$ s. It means $R_n = \infty$ and $\varepsilon = 0$, which is the most serious imbalance. As shown in Fig. 16(a), v_p and v_n are still balanced after R_n is removed, which verifies the full-voltage balancing capability of the proposed scheme. Besides, the modulation signals are basically unchanged. Zero sequence current ($I_0 = 5.25$ A) is injected into the ac side currents, while the amplitude of the latter is halved at half load.

Current waveforms are presented in Fig. 16(b). When R_n is disconnected, the negative pole current decreases to zero instantly, and the required unbalanced current becomes $I_{un} = -I_p$. Fig. 16(b) confirms it is the sum of neutral line current i_{nl} and midpoint current i_{np} that provides the required current, and their steady-state values are well matched with KCL in (37).

The dynamic performance of the proposed control strategy is demonstrated in Fig. 16(c). Through the designed voltage balancing controller, v_{diff} is controlled to zero in less than 0.06 s, with an overshoot of less than 10 V (2.5%). The inner current loop for i_0 also has fast tracking with its reference. As the final output of the controller, m_0 only has a very slight fluctuation during the transient. Moreover, the steady-state value of m_0 is around zero, hence negligible effect on the modulation signals as expected. All of the above complies with the analysis results in Section III-E.

B. Experimental Results

The feasibility and effectiveness of the improved 3L-NPC converter system are also verified by the experimental setup in Fig. 17. A three-phase programmable ac voltage source is used as an ac grid. The zigzag transformer is formed by connecting three single-phase transformers in the way shown in Fig. 10(a). A simple wire is used as the neutral line, which connects the

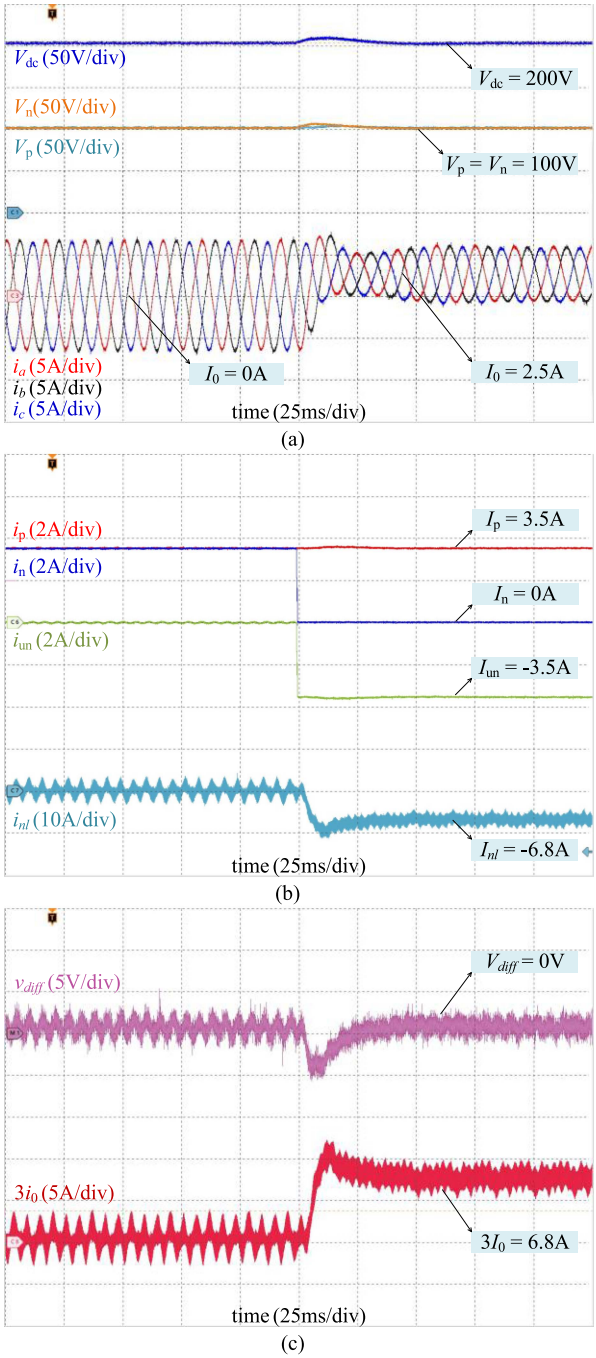

Fig. 19. Experimental waveforms of scenario 2. (a) DC-side voltages and AC-side currents. (b) Current waveforms. (c) Dynamic performance of the controller.

neutral point of a transformer to the midpoint of the dc side. The experimental system is controlled by dSPACE DS1202. Experimental parameters are given in Table III.

Scenario 1 demonstrates that the proposed scheme can balance the pole voltages under a high modulation index ($M = 0.8$). Unbalanced loads ($R_p = 14.4\ \Omega$, $R_n = 28.8\ \Omega$, $\varepsilon = 0.5$) are connected across dc poles from the very start. As shown in Fig. 18, v_{dc} is controlled at its reference value by the dc-link voltage controller. But v_p and v_n cannot be balanced by only relying on

TABLE III
EXPERIMENTAL PARAMETERS

Parameter	Value	Parameter	Value
Grid RMS line voltage	125 V	DC-link voltage	200 V
Grid frequency	60 Hz	Switching frequency	5 kHz
Transformer turns ratio	1.25:1	DC loads (R_p and R_n)	14.4 and 28.8 Ω or 28.8 Ω and ∞
L filter inductance	5 mH	Capacitance per pole	2 mF

the inherent voltage balancing capability of 3L-NPC. When the voltage balancing controller is enabled, a zero sequence current ($I_0 = 2.3$ A) is added into three-phase currents and the pole voltages are quickly balanced.

Scenario 2 demonstrates that the proposed scheme has voltage balancing capability even under the most extreme unbalanced load condition. The dc loads are balanced ($R_p = R_n = 28.8\ \Omega$, $\varepsilon = 1$) initially. Both controllers are enabled from the beginning. In this case, as shown in Fig. 19(a), v_p and v_n are balanced and v_{dc} is kept at 200 V. The injected I_0 is zero. Then, the negative load is disconnected suddenly ($R_p = 28.8\ \Omega$, $R_n = \infty$, $\varepsilon = 0$). With the proposed control strategy, all the voltages reach a steady state after slight fluctuations. Note the current waveforms of i_{abc} are lifted due to the injection of I_0, which is a key feature of the proposed voltage balancing scheme.

The currents in the dc side and neutral line are captured and presented in Fig. 19(b). All current waveforms are in good agreement with those in Fig. 16(b), which validates the correctness of theoretical analysis and simulation results.

To verify the dynamic performance of the proposed scheme, the waveforms of v_{diff} and the sum of zero sequence currents $3I_0$ are captured and shown in Fig. 19(c). It is observed that v_{diff} fluctuates with a magnitude less than 5 V (5%) and returns to a steady state in less than 0.05 s, which validates the fast dynamic characteristic of the designed controller.

V. CONCLUSION

This article presents an improved 3L-NPC converter system for guaranteeing a stable asymmetrical operation of bipolar LVdc grids. Unlike the conventional scheme in Fig. 3, which is based on the injection of zero sequence voltage, the proposed scheme in Fig. 9 is based on the manipulation of zero sequence current. To realize this idea: 1) a zigzag transformer is exploited to prevent the core flux saturation problem; 2) a neutral line is created as the zero sequence current path; 3) controllers are designed to regulate the dc-link voltage and zero sequence current. Since there is no technical limitation for zero sequence current injection, the proposed scheme can ensure voltage balance between dc poles under all the operating conditions.

To verify the proposed converter system and control strategy, simulations are implemented in MATLAB/Simulink. The results validate that the proposed scheme can realize the voltage balance under high modulation index cases and completely unbalanced load conditions. Experimental results obtained from a lab prototype also show good agreement with theoretical and simulation results. Compared with existing schemes, the proposed scheme

not only offers full bipolar voltage balancing capability but also does not require any extra devices or suffer any penalty on component ratings.

REFERENCES

[1] T. Dragičević, P. Wheeler, and F. Blaabjerg, *DC Distribution Systems and Microgrids*. London, U.K.: Inst. Eng. Technol., 2018.

[2] S. Rivera, R. Lizana F., S. Kouro, T. Dragičević, and B. Wu, "Bipolar DC power conversion: State-of-the-art and emerging technologies," *IEEE J. Emerg. Sel. Topics Power Electron.*, vol. 9, no. 2, pp. 1192–1204, Apr. 2021.

[3] G. Van den Broeck, S. De Breucker, J. Beerten, J. Zwysen, M. D. Vecchia, and J. Driesen, "Analysis of three-level converters with voltage balancing capability in bipolar DC distribution networks," in *Proc. IEEE 2nd Int. Conf. DC Microgrids*, 2017, pp. 248–255.

[4] P. Salonen, T. Kaipia, P. Nuutinen, P. Peltoniemi, and J. Partanen, "An LVDC distribution system concept," in *Proc. Nordic Workshop Power Ind. Electron.*, 2008, pp. A3-1–A3-16.

[5] T. Kaipia, P. Salonen, J. Lassila, and J. Partanen, "Possibilities of the low voltage DC distribution systems," in *Proc. Nordic Distrib. Asset Manage. Conf.*, 2006, pp. 1–10.

[6] Y. Gu, W. Li, and X. He, "Analysis and control of bipolar LVDC grid with DC symmetrical component method," *IEEE Trans. Power Syst.*, vol. 31, no. 1, pp. 685–694, Jan. 2016.

[7] G. V. D. Broeck, W. Martinez, M. D. Vecchia, S. Ravyts, and J. Driesen, "Conversion efficiency of the buck three-level DC–DC converter in unbalanced bipolar DC microgrids," *IEEE Trans. Power Electron.*, vol. 35, no. 9, pp. 9306–9319, Sep. 2020.

[8] H. Kakigano, Y. Miura, and T. Ise, "Low-voltage bipolar-type dc microgrid for super high quality distribution," *IEEE Trans. Power Electron.*, vol. 25, no. 12, pp. 3066–3075, Dec. 2010.

[9] J. Lago and M. L. Heldwein, "Operation and control-oriented modeling of a power converter for current balancing and stability improvement of DC active distribution networks," *IEEE Trans. Power Electron.*, vol. 26, no. 3, pp. 877–885, Mar. 2011.

[10] R. Teichmann and S. Bernet, "A comparison of three-level converters versus two-level converters for low-voltage drives, traction, and utility applications," *IEEE Trans. Ind. Appl.*, vol. 41, no. 3, pp. 855–865, May/Jun. 2005.

[11] L. Tan, B. Wu, S. Rivera, and V. Yaramasu, "Comprehensive DC power balance management in high-power three-level DC–DC converter for electric vehicle fast charging," *IEEE Trans. Power Electron.*, vol. 31, no. 1, pp. 89–100, Jan. 2016.

[12] A. Choudhury, P. Pillay, and S. S. Williamson, "Discontinuous hybrid-PWM-based DC-link voltage balancing algorithm for a three-level neutral-point-clamped (NPC) traction inverter drive," *IEEE Trans. Ind. Appl.*, vol. 52, no. 4, pp. 3071–3082, Jul./Aug. 2016.

[13] N. Celanovic and D. Boroyevich, "A comprehensive study of neutral point voltage balancing problem in three-level neutral-point-clamped voltage source PWM inverters," *IEEE Trans. Power Electron.*, vol. 15, no. 2, pp. 242–249, Mar. 2000.

[14] R. M. Tallam, R. Naik, and T. A. Nondahl, "A carrier-based PWM scheme for neutral-point voltage balancing in three-level inverters," *IEEE Trans. Ind. Appl.*, vol. 41, no. 6, pp. 1734–1743, Nov./Dec. 2005.

[15] A. Bendre, G. Venkataramanan, D. Rosene, and V. Srinivasan, "Modeling and design of a neutral-point voltage regulator for a three-level diode-clamped inverter using multiple-carrier modulation," *IEEE Trans. Ind. Electron.*, vol. 53, no. 3, pp. 718–726, Jun. 2006.

[16] S. Rivera, B. Wu, S. Kouro, V. Yaramasu, and J. Wang, "Electric vehicle charging station using a neutral point clamped converter with bipolar dc bus," *IEEE Trans. Ind. Electron.*, vol. 62, no. 4, pp. 1999–2009, Apr. 2015.

[17] L. Tan, B. Wu, V. Yaramasu, S. Rivera, and X. Guo, "Effective voltage balance control for bipolar-DC-bus-fed EV charging station with three-level DC–DC fast charger," *IEEE Trans. Ind. Electron.*, vol. 63, no. 7, pp. 4031–4041, Jul. 2016.

[18] S. Rivera and B. Wu, "Electric vehicle charging station with an energy storage stage for split-DC bus voltage balancing," *IEEE Trans. Power Electron.*, vol. 32, no. 3, pp. 2376–2386, Mar. 2017.

[19] A. Yazdani and R. Iravani, "Three-level, three-phase, neutral-point clamped, voltage-sourced converter," in *Voltage-Sourced Converter in Power Systems: Modelling, Control, and Application*. Hoboken, NJ, USA: Wiley, 2010.

[20] S. Cui, J. H. Lee, J. Hu, R. W. De Doncker, and S. K. Sul, "A modular multilevel converter with a zigzag transformer for bipolar MVDC distribution systems," *IEEE Trans. Power Electron.*, vol. 34, no. 2, pp. 1038–1043, Feb. 2019.

[21] C. Perera, J. Salmon, and G. J. Kish, "Multiport converter with independent control of AC and DC power flows for bipolar DC distribution," *IEEE Trans. Power Electron.*, vol. 36, no. 3, pp. 3473–3485, Mar. 2021.

[22] M. P. Kazmierkowski and L. Malesani, "Current control techniques for three-phase voltage-source PWM converters: A survey," *IEEE Trans. Ind. Electron.*, vol. 45, no. 5, pp. 691–703, Oct. 1998.

Bowei Li (Graduate Student Member, IEEE) received the B.S. and M.S. degrees in electrical engineering from Shandong University, Jinan, China, in 2017 and 2020, respectively. He is currently working toward the Ph.D. degree in energy system with the Department of Electrical and Computer Engineering, University of Alberta, Edmonton, AB, Canada.

His research interests include topology, control, and power quality of the dc distribution system.

Hao Tian (Member, IEEE) received the B.S. and M.Eng. degrees in electrical engineering from Shandong University, Jinan, China, in 2011 and 2014, respectively, and the Ph.D. degree in energy system from the University of Alberta, Edmonton, AB, Canada, in 2019.

After that, he was a Postdoctoral Research Fellow with the University of Alberta until 2022. Since 2023, he has been a Full Professor with Shandong University, Jinan, China. His research interests include multilevel topology and PWM, high-power converter control, and power quality of hybrid ac–dc microgrids.

Li Ding (Member, IEEE) received the B.Eng. degree from Shanghai University, Shanghai, China, in 2013, the M.Sc. degree from the Harbin Institute of Technology, Harbin, China, in 2015, and the Ph.D. degree from the University of Alberta, Edmonton, AB, Canada, in 2020, all in electrical engineering.

He is currently a Postdoctoral Research Fellow with the Department of Electrical and Computer Engineering, University of Alberta, Edmonton, AB, Canada. His research interests include current-source converters, sensorless motor drives, multilevel converters, and hybrid ac/dc networks.

Xuesong Wu (Member, IEEE) received the B.Eng. (Yisheng Mao Honors) and M.Sc. degrees in electrical engineering from Southwest Jiaotong University, Chengdu, China, in 2016 and 2019, respectively. He is currently working toward the Ph.D. degree in energy system with the Department of Electrical and Computer Engineering, University of Alberta, Edmonton, AB, Canada.

His research interests include electrical machine drives and grid-tied inverters.

Gregory J. Kish (Senior Member, IEEE) received the B.E.Sc. degree from the University of Western Ontario, London, ON, Canada, in 2009, and the M.A.Sc. and Ph.D. degrees from the University of Toronto, Toronto, ON, Canada, in 2011 and 2016, respectively, all in electrical engineering.

He is currently an Associate Professor with the University of Alberta, Edmonton, AB, Canada. His research interests include the development and application of power electronic converter systems in electric grids.

Yunwei Ryan Li (Fellow, IEEE) received the B.Sc. in Engineering degree in electrical engineering from Tianjin University, Tianjin, China, in 2002 and the Ph.D. degree from Nanyang Technological University, Singapore, in 2006.

In 2005, he was a Visiting Scholar with Aalborg University, Aalborg, Denmark. From 2006 to 2007, he was a Postdoctoral Research Fellow with Ryerson University, Toronto, ON, Canada. In 2007, he was with Rockwell Automation Canada, Edmonton, AB, Canada, before he joined University of Alberta, Edmonton, AB, Canada, in the same year. Since then, he has been with the University of Alberta, where he is currently a Professor. His research interests include distributed generation, microgrid, renewable energy, high power converters, and electric motor drives.

Dr. Li is currently the Vice President for Products of IEEE Power Electronics Society (PELS). He was an Editor-in-Chief for the IEEE TRANSACTIONS ON POWER ELECTRONICS LETTERS during 2019–2023. He was an Associate Editor for the IEEE TRANSACTIONS ON POWER ELECTRONICS, IEEE TRANSACTIONS ON INDUSTRIAL ELECTRONICS, IEEE TRANSACTIONS ON SMART GRID, and IEEE JOURNAL OF EMERGING AND SELECTED TOPICS IN POWER ELECTRONICS. He was the General Chair of IEEE Energy Conversion Congress of Exposition (ECCE) in 2020. He is theAdCom Member at Large for IEEE Power Electronics Society (PELS) 2021–2023. He was the recipient of the Nagamori Foundation Award in 2022 and the Richard M. Bass Outstanding Young Power Electronics Engineer Award from IEEE PELS in 2013. He is recognized as a Clarivate Highly Cited Researcher.